18TH WORLD CONFERENCE ON EARTHQUAKE ENGINEERING
WCEE2024
MILAN

MILAN, ITALY
30TH JUNE - 5TH JULY 2024

www.wcee2024.it

HIGHER-MODE RESPONSE OF BRACED FRAMES WITH ELASTIC SPINES SUBJECTED TO MODAL PUSHOVER ANALYSIS.

Bryam Astudillo[1] & Barbara Simpson, Ph.D.[2]

[1] Graduate Research Assistant, Department of Civil and Environmental Engineering, Stanford University, bryam.astudillo@stanford.edu

[2] Assistant Professor, Department of Civil and Environmental Engineering, Stanford University, bsimpson@stanford.edu

Abstract: *Advancements in seismic hazard mitigation and resilience have spurred the exploration and development of lateral-force resisting systems with enhanced performance goals. In this context, brace frames coupled with elastic spines offer a more uniform drift distribution with building height that reduces the concentration of damage in a few stories and therefore reduces the likelihood of a story mechanism. However, properly sizing the spine, along with selecting and placing the energy dissipators, remains challenging and lacks standardized procedures due to 1) the kinematic and force compatibility between the pivoting spine and the energy dissipators and 2) the near-elastic higher-modes demands that are present in this type of system; both closely governed by the selection of the spine strength and stiffness. This study investigates the nonlinear static response of 8-story Strongback Braced Frames (i.e., brace frames where the elastic spine is composed of a pivoting truss called strongback) using a first and second-mode force pattern. The archetypes have different variations in the implementation of the strongback; e.g., keeping the strongback in a separate bay from the main brace frame or embedding the strongback into the frame. In pushing the archetypes with a first-mode force pattern, the strongback imposes more uniform drifts, without a significant increase in the system's ultimate capacity. In pushing with a second-mode force pattern, the strongback delays the formation of a mechanism and increases the system's ultimate capacity to values comparable to expected elastic demands under MCE intensities. The distribution of story shears between the main frame and the strongback is assessed, and the implications of higher-mode demands in sizing the brace and ties of the strongback are highlighted. It is expected that results from this paper may begin to inform future code-based provisions in adopting the use of near-elastic spines in enhanced performance systems.*

1 Introduction

Braced frames were proposed several decades ago; e.g., Eccentrically Braced Frames (EBF) (Roeder and Popov, 1978), Concentrically Braced Frames (CBF) (Khatib et al., 1988), Buckling Restrained Braced Frames (Watanabe et al., 1988; Fujimoto et al., 1990). Although such systems satisfy modern performance requirements, such as Life Safety or Collapse Prevention metrics established in AISC 341 (2022), ASCE-7 (2022), ASCE-41 (2017) or P-695 (2009), braced frame systems are known to concentrate damage in a few stories, increasing the probability of large peak drifts and potentially increasing the probability of structural instabilities. Many have suggested strategies to reduce such drift concentrations by imposing a more uniform drift distribution across the building height, where the overall peak drifts are reduced with some increases in drifts in other stories. For example, stiff pivoting elements, herein referred to as spines, can be introduced to re-distribute shear demands across stories by providing an elastic load path (Tremblay, 2003; MacRae et al., 2004; Lai and Mahin, 2015). However, adding such spines to the frame tends to alter the distribution of story shears in the full system and increase the contributions of higher-mode effects to the system response (Wiebe and Christopoulos, 2015; Simpson, 2020). A practical understanding of the behavior in systems attached to

spines is essential so that particularities, such as higher-mode effects, are appropriately considered in developing practical methods for design.

Pivoting spines have been studied by many authors under different names and variations. Some uses of pin-based elastic components used to enforce a uniform drift profile include continuous columns (MacRae et al., 2004; Ji et al., 2009; Flores et al., 2016), pinned-base shear walls (Qu et al., 2012), and braced frames used as elastic trusses (Tremblay and R, 2003; Takeuchi and Suzuki, 2003; Qu et al., 2014; Lai and Mahin, 2015). For example, in combining an elastic truss with a BRBF as shown in Figure 1(b)-(c), the elastic portion of the braced frame formed by braces and ties can be interpreted as a spine, sometimes referred to as a strongback (Lai and Mahin, 2015) and later the combined system as a Strongback Braced Frame (SBF). The effectiveness of pivoting spines in imposing more uniform drifts has been supported experimentally (Slovenec et al., 2017; Simpson and Mahin, 2018; Fahnestock et al., 2021). However, numerical and experimental results have also shown that the forces in the spines are not limited by a mechanism in all modes and can exhibit large force demands attributed to near-elastic higher-mode effects (Simpson, 2020; Astudillo et al., 2023). This higher-mode characteristic is distinct from other systems like CBFs, EBFs, and BRBFs, where the force demands are often well-constrained by the formation of a mechanism in all modes.

Although many have proposed design methods for proportioning the spine, design practitioners lack standardized procedures that could facilitate the adoption of spines. Challenges in adequately proportioning arise from: (i) determining the stiffness required on the spine to mitigate drift concentrations, (ii) distributing the story shear between the main frame and the spine in a practical manner, and (iii) addressing the demands imposed by near-elastic higher-mode force demands. For (i), similar approaches developed by several authors could be adapted to inform the required stiffness to mitigate drift concentrations, e.g., (MacRae et al., 2004). For (ii), a combined shear and flexural beam analogy could inform the story shear distribution (Khan and Sbarounis, 1964; Heidebrecht and Smith, 1973; Miranda, 1999; Palermo et al., 2018). However, solutions proposed for (i) and (ii) typically only consider a first-mode response, while observations consistent with (iii), illustrate the need to extend such formulations to account for near-elastic higher-mode demands (Wiebe and Christopoulos, 2015; Chen et al., 2017; Simpson and Rivera Torres, 2021).

Additional considerations are needed for systems that are coupled with spines and therefore exhibit a near-elastic higher-mode response. This study compares the behavior of three 8-story BRBFs with and without a strongback. The force redistribution is characterized between the main frame and the spine when first and higher-mode inertial force distributions are considered; herein, the focus is on a first- and second-mode force pattern. Results show that the inclusion of a strongback reduces peak drift demands and reduces the likelihood of concentrating damage in a few stories. However, the distribution of story shear depends on the loading profile. Although the strongback is not expected to be subjected to a large story shear nor provide additional system capacity in a first-mode response, the strongback is subjected to large story shear demands and large system strength capacity in the second mode. Finally, the side effects of increasing the capacity under higher-mode force patterns are noted by inspecting the axial force and bending moment demands in each member.

2 Modal pushover analysis

The interactions of the strongback with the main frame (i.e., the Buckling Restrained Braced Frame, BRBF), considering different lateral force patterns, were studied for a reduced number of representative archetypes using the results from modal pushover analyses (Chopra and Goel, 2002; Chopra et al., 2004). Each archetype was analyzed under the application of an incremental lateral load pattern proportional to s_n:

$$s_n = \Gamma_n m \phi_n \tag{1}$$

where s_n represents the distribution of the inertial force given the mass distribution $\boldsymbol{m}$, the n^{th} mode of vibration ϕ_n, and a scalar factor Γ_n computed with Equations 2, 3, and 4 (Chopra, 2007):

$$\Gamma_n = L_n^h / M_n \tag{2}$$

$$L_n^h = \sum_{j=1}^{N} m_j \phi_{jn} \quad (3)$$

$$M_n = \sum_{j=1}^{N} m_j \phi_{jn}^2 \quad (4)$$

The archetypes were pushed with a force pattern s_n until the system exhibited structural instability (e.g., a mechanism) or exceeded a reference target of interest derived from the linear elastic response of a single-degree-of-freedom oscillator and a given design spectrum. Such targets encompassed the contributions of each mode ϕ_n to the elastic roof drift ratio ($\theta_{r,e}$) and the elastic base shear ($V_{b,e}$) as given per $\theta_{r,e,n}$ and $V_{b,e,n}$ below:

$$\theta_{r,e,n} = \Gamma_n \phi_{rn} D_n / H \quad (6)$$

$$V_{b,e,n} = m_n^* A_n \quad (7)$$

where $m_n^* = \Gamma_n L_n^h$ is the effective modal mass, H is the building height, and D_n and A_n are the spectral pseudo-displacement and pseudo-acceleration at the Design Earthquake (DE) or Maximum Considered Earthquake (MCE) intensities (i.e., $S_a(T_n)$ and $1.5S_a(T_n)$, respectively). Although the values for $\theta_{r,e,n}$ and $V_{b,e,n}$ do not consider nonlinear effects, they were considered useful in providing the reader with reference magnitudes of expected drifts and shear demands for a linear elastic system.

Using modal pushover analysis, this study focused on the first two modes of vibration to investigate the pivoting motion of the strongback under first-mode lateral forces s_1 and the flexural behavior of the strongback under second-mode lateral forces s_2. Then, several criteria were compared between the archetypes, including 1) base shear capacity, 2) story drift concentration, 3) plastic deformation, 4) story shear distribution between the main frame and the strongback, and 5) axial force and bending moment demands. The plastic deformation occurring in key members, the braces, beams, and columns was compared to the reference values in ASCE 41-17 (ASCE-41, 2017) and categorized according to acceptance criteria for Immediate Occupancy (IO), Life Safety (LS), Collapse Prevention (CP).

3 Archetypes

Three 8-story archetypes were selected for the study. One archetype does not have any strongback while the other two have different implementations of the strongback: Archetype A represents a typical Buckling Restrained Braced Frame (BRBF), Archetype B represents a BRBF attached to a pivoting strongback located in a separate bay, and Archetype C represents a BRBF with a strongback embedded into the main frame. The archetypes were designed using a common building plan and location.

3.1 Building layout and design parameters

The archetype building assumed a regular building plan with high gravity loads and a penthouse on the roof with seismic risk category II. The total seismic weight of the building was $W_{eff} = 14{,}494$ kip. Half of the weight, $W = 7247$ kip was used to size a representative line of lateral-force resisting frames in a two-dimensional space. Typical bay width ($b = 30ft$) and story heights ($h_j = 15\ ft$) were assumed, with a taller first story of $h_1 = 18\ ft$. The archetypes were sized for a design spectrum defined by $S_{DS} = 1.40$, $S_{D1} = 0.63$. These spectral pseudo-accelerations are consistent with (Simpson, 2020), which modified the values from the Seismic Design Category D_{MAX} in FEMA P695 (P-695, 2009) to account for scaling of the ground motions at the higher-mode periods.

Seismic design parameters were consistent with the values listed for Buckling Restrained Braced Frames (BRBF) (ASCE-7, 2016); e.g., a response modification coefficient $R = 8$ was assumed for the first-mode response with an estimated upper-limit period $C_u T_a = 1.55s$. The Seismic Response Coefficient C_s used to compute the design base shear V_b was dominated by the minimum threshold $C_{s,min}$.Table 1, summarize the dynamic properties and shear values for the BRBF and are later used as reference points to contrast with the modal pushover results.

Table 1. Reference properties and estimated demands for the BRBF.

Parameter		ASCE-7[1]	Modal response		
			Mode1	Mode2	
Dynamic Properties	T_n	1.55	1.90	0.65	s
	m_n^*	1.00	0.74	0.19	-
	W_{eff}	7247	5358	1350	kip
Elastic Response at DE	$S_a(T_n)$	0.41	0.33	0.97	g
	$V_{b,e,i}$	2971[2]	1776	1308	kip
	$\theta_{r,e,mi}$		0.011	0.002	rad
Nonlinear response at DE	$S_a(T_n)/R$	0.05[3]	0.04	0.12[4]	g
	$V_{b,e,i}/R$	371[3]	222	164[4]	kip

[1]Base shear, neglecting $C_{s,min}$.

[2]$V_{b,e,m1}$, elastic value used for reference; it is not expected to be reached.

[3]Archetype designs considered $C_s = C_{s,min} = 0.061$ g and $V_b = 444$ kip.

[4] R is not expected to be 8 in the higher-mode response of systems with spines

3.2 Braced frame configurations

Three brace configurations were studied; see the element layout and sizes in Figure 1Figure 1. Archetype A represents a typical Buckling Restrained Braced Frame (BRBF) with 2-story-X-bracing, while Archetypes B and C represent alternate BRBF configurations in which a strongback with W14 braces is included. Archetype B considers a strongback separate from the main BRBF and connected via idealized pin-ended collectors that do not constrain the pivoting motion of the strongback. Archetype C achieves embedding the strongback into the BRBF by considering the X-bracing with one side compound of BRBs and the other side compound of the W-braces of the strongback; in this configuration, the beam extends continuously across the floor providing flexural stiffness that constrains the pivoting motion of the strongback in some extend and splits the strongback tie from floor-to-floor.

Archetype A was sized using Equivalent Lateral Force (ELF) and capacity-limited design, Archetype B used the same sections as Archetype A for the main frame while the strongback was sized using modal pushover analysis, and, Archetype C used the sections from (Simpson and Rivera Torres, 2021) which were selected with iterative nonlinear dynamic analysis.

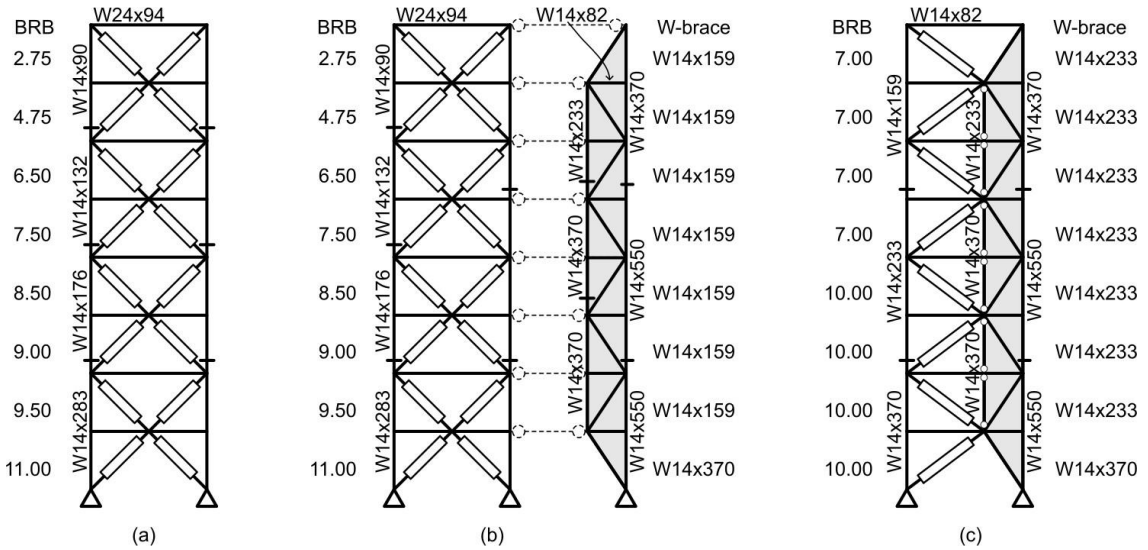

Figure 1. 8-story braced frame configurations with X-bracing layout: a) BRBF with no strongback, Archetype A; b) BRBF with separate strongback, Archetype B; c) BRBF with embedded strongback, Archetype C. BRBs size is given by the core area A_{sc} in in^2.

3.3 Numerical Models

Two-dimensional numerical models were created in OpenSeesPy (McKenna et al., 2010; Zhu et al., 2018). A similar modeling approach was adopted for all the archetypes. Figure 2 shows the schematic for the numerical model of Archetype C as a reference; a detailed description can be found in the appendix of (Simpson, 2020). The flexural contribution of the continuous gravity framing was neglected.

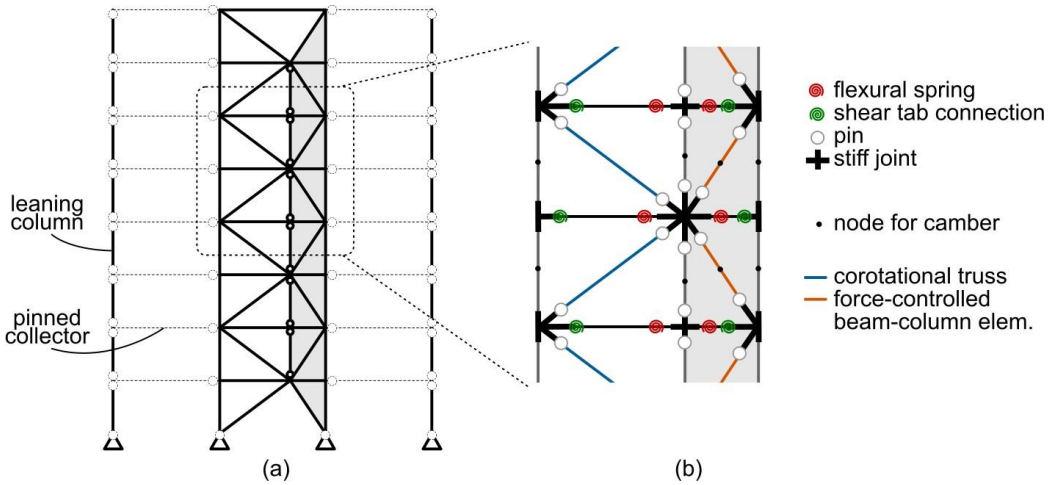

Figure 2 Schematic of the numerical model. a) global view and b) close-up view

4 First-Mode response

The response from nonlinear static analysis, using $\mathbf{s}_1$, is compared across the three archetypes.

4.1 Pushover curve

Figure 3(a) shows the roof drift ratio versus the base shear for the three archetypes under the force pattern $\mathbf{s}_1$; in the figure, story drift ratios are also plotted to visualize the concentration of drift in some stories. In pushing the models using $\mathbf{s}_1$, the archetypes had an ultimate base shear capacity consistent with the design base shear and system overstrength, despite the presence of the strongback in Archetype B and C. Archetype A shows a reduction of capacity due to a story mechanism in the lower stories, along with large P-Delta effects induced by the drift concentration. Figure 3(a) also contains markers denoting the reference point for the snapshots presented hereafter; a roof drift ratio of 0.02 rad was selected based on the expected drift ratios under the excitation at the DE intensity.

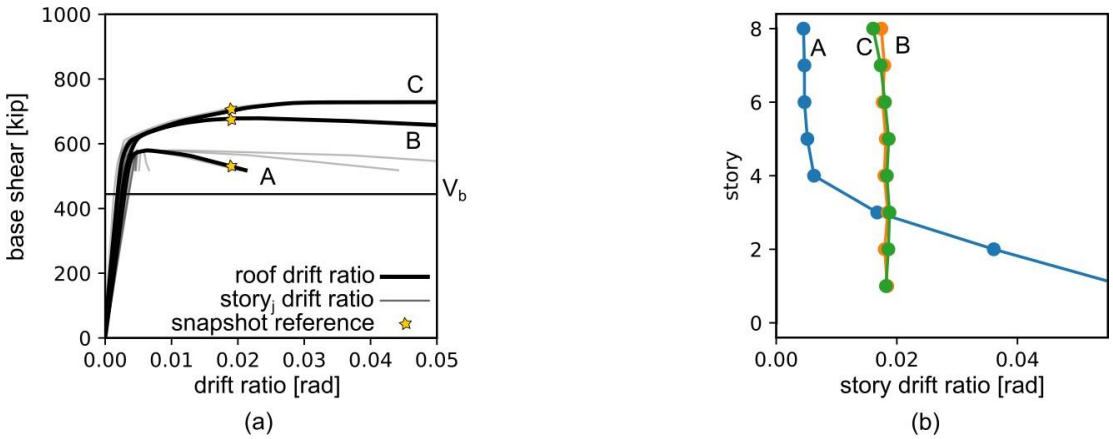

Figure 3 First-mode pushover under s_1. a) Roof drift ratio versus base shear and b) story drift ratios at point of reference.

4.2 Displaced shape and plastic deformations

Figure 3(b) shows the story drift ratio profile at the roof drift ratio of reference. In the case of archetype A, the plot reflects drifts close to the point of structural instability (roof drift ratio 0.02 rad. with story drift ratios beyond 0.05 rad.). Noticeably from Figure 3(b), the drift concentration on Archetype A led to a large story drift ratio in

the lower stories with small drifts in the upper stories. For the other archetypes, there is a more uniform drift distribution across stories due to the presence of the strongback.

Figure 4 shows the archetypes' displaced shape and plastic deformations at the point of reference. The structure elements are color-coded to reflect the relative amount of plastic deformation in relation to the acceptance criteria listed in ASCE 41-17 (ASCE-41, 2017) (i.e., IO, LS, CP, and beyond). Archetype A exhibited high plastic demands in the bottom braces (beyond CP) while the upper braces remained elastic. Although the BRBs were able to withstand large plastic strains, large strains are undesirable to mitigate low-cycle fatigue. Archetype B exhibited similar plastic demands across the BRBs of all stories implying a more efficient utilization of all of the BRBs; all BRBs fall in the LS category. The W-braces remained elastic. Observations for Archetype C are similar to Archetype B.

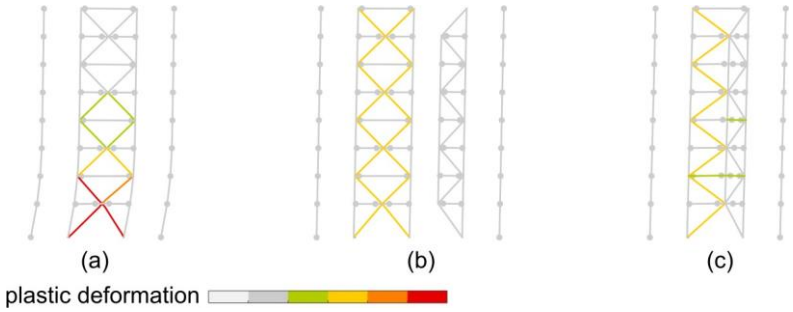

Figure 4 First-mode plastic deformation for a) Archetype A, b) Archetype B, c) Archetype C

4.3 Story shear distribution

The story shear was distributed between the inelastic and elastic elements (i.e., columns, beams, braces, leaning columns). Figure 5 illustrates the total story shear and the amounts resisted by the BRBs and W-braces at the point of reference; consistently, Figure 6 shows the distribution of the story shear to all the elements of the seismic-force resisting system with diagrams showing the magnitude of the force in the global x-direction resisted by each element.

For Archetype A (Figure 5 (a)), the story shear was resisted by the BRBs in each story with small amounts of shear resisted by the columns. The difference between the total story shear and the shear going into the BRBs is attributed to the pronounced P-Delta effects resulting from the drift concentration. For Archetype B (Figure 5(b)), the story shear was mostly resisted by the BRBs in each story, while the pivoting strongback only attracted minor shear demands compared to the BRBs. For Archetype C (Figure 5(c)), the story shear was resisted by both the BRBs of the main frame and the W-braces of the strongback. The kinematics of the strongback and main frame do not interact as much in Archetype B compared to Archetype C.

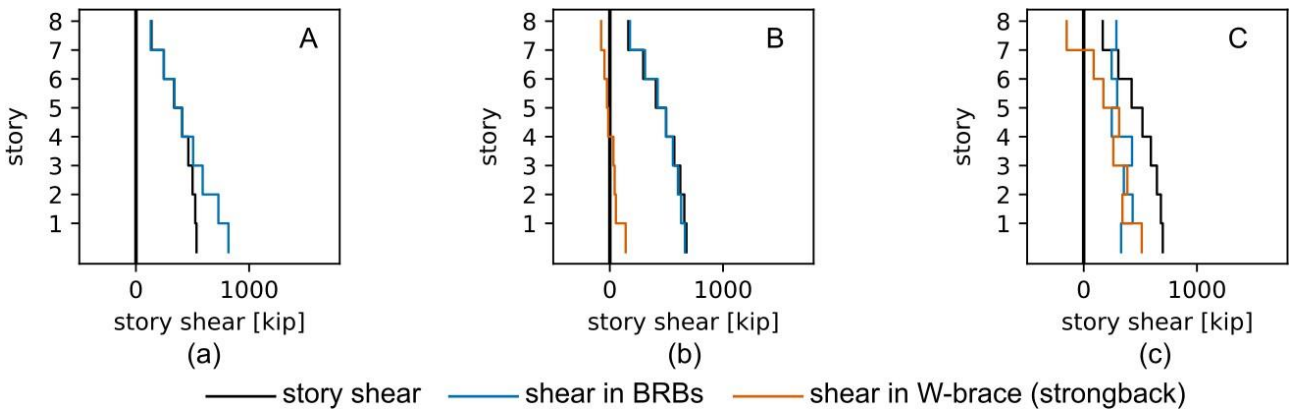

Figure 5 First-mode story shear distribution. A) Archetype A, b) Archetype B, c) Archetype C.

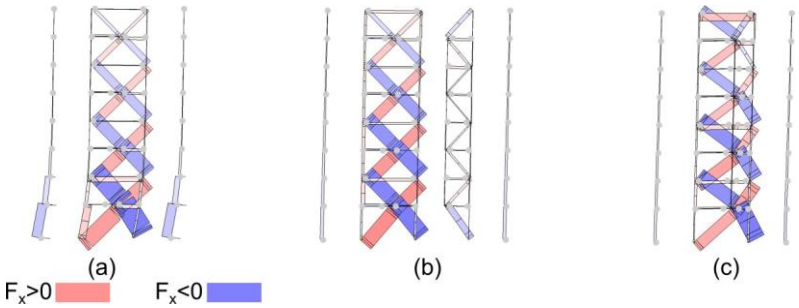

Figure 6 Force-mode Force component in the global-x-direction, F_x, for a) Archetype A, b) Archetype B, c) Archetype C.

4.4 Axial force and bending moment diagrams

The axial-force diagrams of the archetypes are illustrated in Figure 7**Error! Reference source not found.**. Archetype A shows the tension and compression of the column on the left and right of the frame, respectively, due to the forces delivered by the BRBs and the overturning moment in the building. Columns in the main frame of Archetype B behave in a similar manner, while the pivoting strongback receives loads from mostly gravity loading as the collector was assumed to be pin-ended and the W-brace did not take much load. Archetype C shows tension in the left column, and compression on the strongback tie and most-right column due to the overturning moment and vertical component of the braces. Also, note that any loading in the strongback tie needs to be transmitted to the ground through the first-story elastic brace.

The bending moment diagram Is illustrated in Figure 8. Archetype A exhibits large moment demands due to the drift concentration in the lower stories while Archetypes B and C exhibit fewer moment demands in the columns with a better distribution of demands across multiple stories. The moment diagram in Archetype C highlights the intended uplift of the tie resisted by the continuous beam.

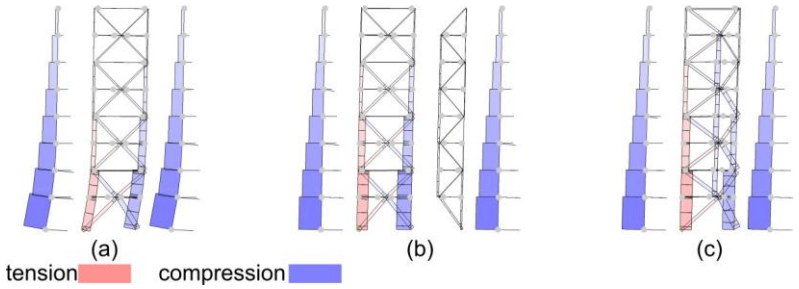

Figure 7 First-mode axial force diagram for a) Archetype A, b) Archetype B, c) Archetype C.

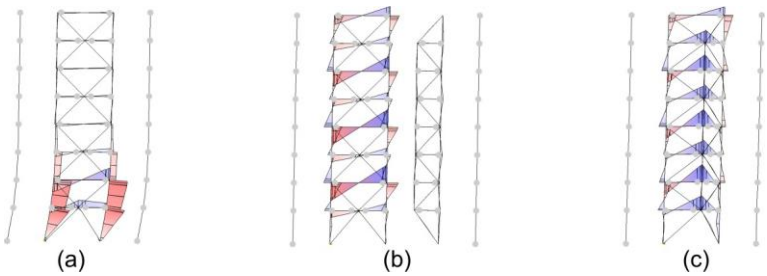

Figure 8 First-mode bending moment diagram for a) Archetype A, b) Archetype B, c) Archetype C.

5 Second-Mode response

The response from nonlinear static analysis, using $\mathbf{s_2}$, is compared across the three archetypes.

5.1 Pushover curve

The roof drift ratio versus story shear using the $\mathbf{s_2}$ force pattern is illustrated in Figure 9(a). Estimated contributions of the second-mode response to the total base shear, as noted in Table 1, are overlapped on the plots; for example, the second-mode base shear that coincides with an elastic base shear response for the DE and MCE (i.e., $V_{b,e,m2}$ and $1.5V_{b,e,m2}$). Reference points for all snapshots are highlighted in the plot.

Archetype A exhibits the least base shear capacity among the archetypes under s_2; i.e., the demands that could arise in this system given a purely second-mode response are limited by a mechanism and well below the reference value for elastic response under DBE or MCE. Archetypes B and C, with the strongback, exhibit a less pronounced nonlinear response under this loading condition, with base shear capacities that exceeded the elastic shear demands expected from DE and MCE events; i.e., given a purely second-mode response, archetypes B and C are expected to have a near-elastic response characterized by some inelastic behavior but with a near-linear force-displacement relationship at the system level.

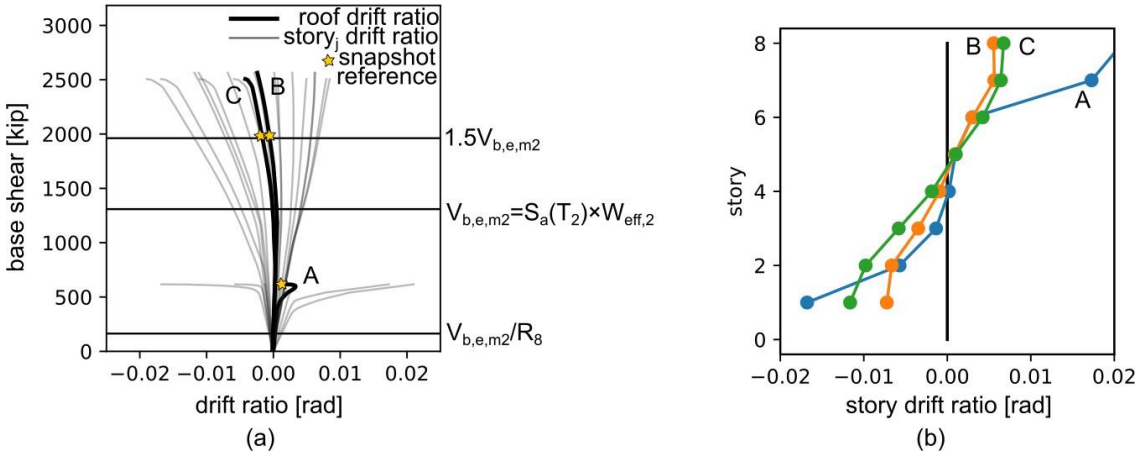

Figure 9 Second-mode pushover considering s_2. a) Roof drift ratio vs base shear, and b) story drift ratios at the point of reference

5.2 Displaced shape and plastic deformations

Figure 9(b) shows the story drift ratio profile at the point of reference. All archetypes tend to have larger drifts in the bottom and upper stories due to the second-mode shape. However, Archetype A concentrates the largest drifts at the upper stories due to a mechanism. As the stiffer archetype, Archetype B tends to have the lowest peak drift ratios (below 0.01 rad), while Archetype C shows intermediate drifts at the bottom stories while maintaining a similar drift ratio to Archetype B in the upper stories.

The displaced shape and plastic deformations in the three archetypes at the points of reference are presented in Figure 10. Archetype A exhibits high plastic deformations in the BRBs located in the upper and bottom stories, with values consistent with LS. Archetype B exhibits low plastic deformations in the BRBs located in the upper and bottom stories, with values corresponding to IO. Archetype C exhibits moderate and low plastic deformation in the BRBs located in the upper and bottom stories, respectively; the lower-story braces reached the LS acceptance criteria while others remained at IO. For Archetypes B and C, the elements of the strongback remained in the elastic range.

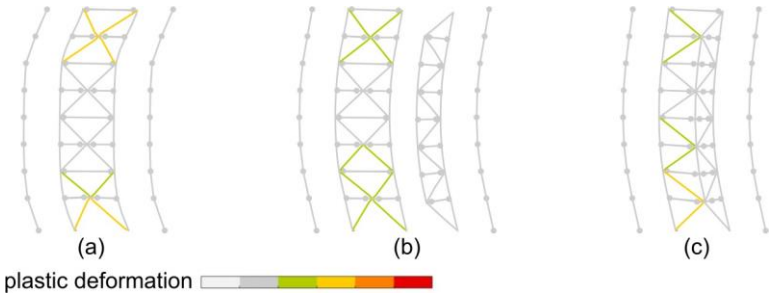

Figure 10 Second-mode plastic deformation for a) Archetype A, b) Archetype B, c) Archetype C.

5.3 Story shear distribution

The story shear given the second-mode load pattern is presented in Figure 11; the plots show the total story shear and the contributions of the BRBs and W-braces at the point of reference. The force component in the global-x-direction resisted by each element is presented in Figure 12; the amount of force shown in the diagrams is related to how much of the story shear is resisted by a given element.

The BRBs in Archetype A take all the story shear that arrives at the upper and bottom stories due to s_2. For Archetype B, the story shear is shared between the BRBs and the W-braces. The participation of the strongback during a second-mode pushover is significantly different from a first-mode pushover, where the pivoting strongback previously did not take much load and the mechanism occurred after yielding the BRBs. In a second-mode pushover, after yielding of the BRBs, the strongback is still able to resist the imposed forces without forming a mechanism. After yielding of some of the BRBs in some stories, the excess shear is resisted by the W-braces. If the strongback is designed to remain elastic, the W-braces must be designed to resist these large higher-mode force demands. Note, although the BRBs resist some of the story shear, given the relatively smaller size of the upper story BRBs designed for only the $\mathbf{s_1}$ force pattern, the demands in the upper W-braces are close to the total elastic story shear V_j. Archetype C exhibits a similar response to Archetype B, where the strongback takes a significant amount of shear while the shear taken by the BRBs is limited by their adjusted capacity based on their strains.

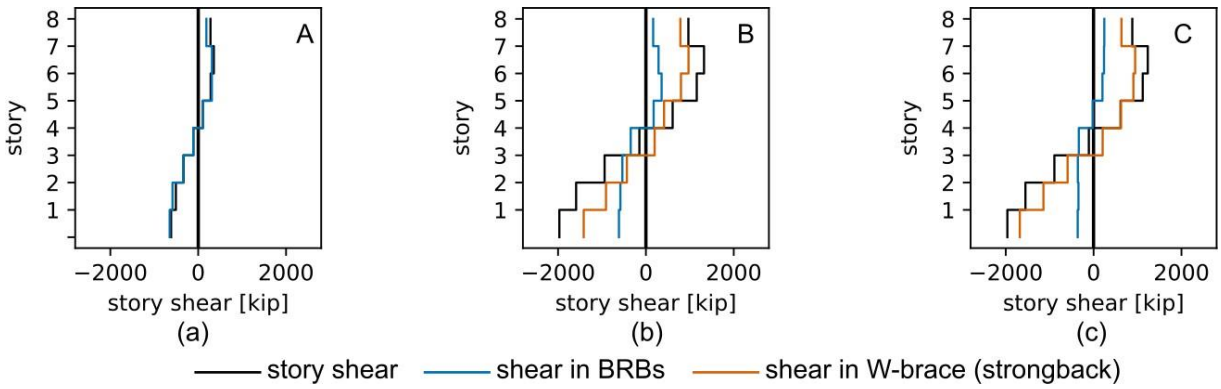

Figure 11 Second-mode story shear distribution. a) Archetype A, b) Archetype B, c) Archetype C.

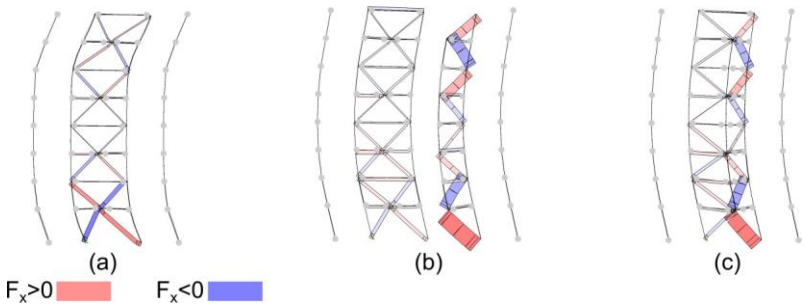

Figure 12 Second-mode force component in the global-x-direction, F_x, for a) Archetype A, b) Archetype B, c) Archetype C.

5.4 Axial force and bending moment diagrams

The axial force diagram at the point of reference is presented in Figure 13. For Archetype A, the axial demands in the BRBF columns are limited by the capacity of the BRBs. For Archetype B, the BRBF columns are similarly limited as Archetype A. However, in Archetype B, the ties of the strongback carry a significant amount of axial demands, which are in accordance with the diagrams expected from the chords of a simply supported truss loaded in single bending. Given the direction of the push, the left tie is in tension, and the right tie is in compression. For Archetype C, even though it is embedded, the strongback experiences similar axial force demands to Archetype B. Since the strongback is designed to remain elastic and as there is no mechanism occurring up to the reference point in Archetypes B and C, the magnitude of the force demands correspond to the elastic ordinates of the design spectrum for a second-mode response.

The bending moment diagram at the point of reference is presented in Figure 14. For Archetype A, the columns show a large bending moment due to drift concentrations in the upper and lower stories. For Archetype B, the ties of the strongback exhibit large moments because of its continuity. For Archetype C, the left tie of the strongback does not exhibit moments as the tie was split by the continuous beam and assumed to be pinned from floor to floor; the right tie, which was a continuous column, exhibits large moments that should be considered in designing the archetype under second-mode effects. For both Archetypes B and C, the strongback behaves like a simply supported truss or an equivalent beam in flexure under $\boldsymbol{s_2}$.

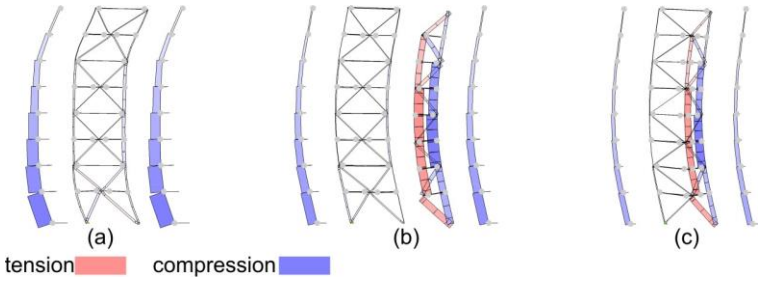

Figure 13 Second-mode axial force diagram for a) Archetype A, b) Archetype B, c) Archetype C.

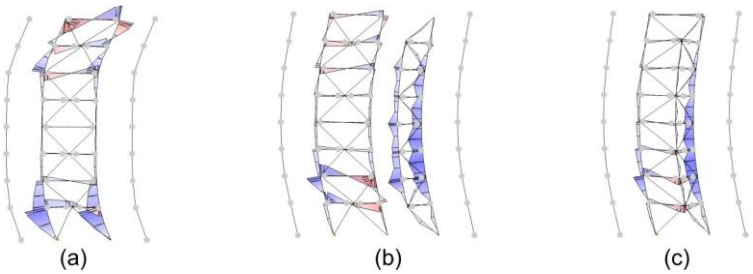

Figure 14 Second-mode bending moment diagram for a) Archetype A, b) Archetype B, c) Archetype C.

6 Conclusions

To understand the effects of including a strongback and the interactions between the system elements, three 8-story archetypes were studied using modal pushover analysis. One archetype lacked a strongback, while the other two featured different strongback implementations. Archetype A represented a typical Buckling Restrained Braced Frame (BRBF), Archetype B featured a BRBF attached to a pivoting strongback located in a separate bay, and Archetype C represented a BRBF with an embedded strongback where one side of the braces consisted of BRBs and the other side of W-shape braces linked through a tie. The archetypes were modeled in OpenSeesPy and subjected to various load patterns, simulating first-mode and second-mode responses. Several criteria were compared, including base shear capacity, story drift concentration, plastic deformation in the elements, story shear distribution between the main frame and the strongback, and axial force and bending moment demands.

Given a first-mode force pattern, the pivoting strongback is shown to reduce the drift concentrations through a more uniform drift profile. The system's capacity in the first mode was consistent with the design base shear including overstrength. Under such loading conditions, the story shear in the pivoting strongback was minimal compared to the shear of the BRBs, with the shear in the strongback increasing when the pivoting is constrained. Given a second-mode force pattern, although the drifts were not expected to be uniform, the strongback avoided a concentration of drifts; however, contrary to the first loading condition, the system capacity exceeded the elastic demands calculated at the MCE intensity level at the second-mode period. Under the second loading condition, the strongback attracted a considerable amount of shear, exceeding the shear resisted by the BRBs and resulting in large axial force and bending moments demands to the strongback ties. These results are in agreement with the near-elastic higher-mode effects observed in systems with strongbacks and provide a practical understanding of such effects towards a more comprehensive design of these systems.

7 Acknowledgments

This research investigation is funded by the U.S. National Science Foundation under the project Collaborative Research: Frame-Spine System with Force-Limiting Connections for Low-Damage Seismic-Resilient Buildings (CMMI 1928906, 1926326, and 1926365); the authors sincerely thank Professor Larry Fahnestock, Professor Richard Sause, Professor James Ricles, and Jessica Duke for their valuable inputs and discussions as part of the aforementioned project. Additional support is provided by the American Institute of Steel Construction and by the Shah Fellowship on Catastrophic Risk at Stanford University. Any opinions, findings, conclusions, or recommendations expressed in this paper are those of the authors and do not necessarily reflect the views of the above-mentioned participants or funding sources.

8 Conflict of Interest

The authors declare no conflicts of interest.

9 Data availability statement

Some or all data, models, or scripts that support the findings of this study are available from the corresponding author upon reasonable request.

10 References

ANSI/AISC 341 (2022). *Seismic Provisions for Structural Steel Buildings*. American Institute for Steel Construction, Chicago, IL.

ASCE-41 (2017). *Seismic Evaluation and Retrofit of Existing Buildings*. American Society of Civil Engineers, Reston, VA.

ASCE-7 (2016). *Minimum Design Loads and Associated Criteria for Buildings and Other Structures*. American Society of Civil Engineers, Reston, VA.

ASCE-7 (2022). *Minimum Design Loads and Associated Criteria for Buildings and Other Structures*. American Society of Civil Engineers, Reston, VA.

Astudillo, B., Rivera, D., Duke, J., Simpson, B., Fahnestock, L., Sause, R., Ricles, J., Kurata, M., Okazaki, T., Kawamata, Y., Tao, Z., and Qie, Y. (2023) 'Modeling uncertainty of specimens employing spines and force-limiting connections tested at E-defense shake table', *Earthquake Engineering & Structural Dynamics*, p. eqe.3976. Available at: https://doi.org/10.1002/eqe.3976.

Chen, X., Takeuchi, T., and Matsui, R. (2017). Simplified design procedure for controlled spine frames with energy-dissipating members. *Journal of Constructional Steel Research*, 135:242–252.

Chopra, A. K. (2007). *Dynamics of structures*. Pearson Education India.

Chopra, A. K. and Goel, R. K. (2002). A modal pushover analysis procedure for estimating seismic demands for buildings. *Earthquake Engineering Structural Dynamics*, 31(3):561–582.

Chopra, A. K., Goel, R. K., and Chintanapakdee, C. (2004). Evaluation of a modified mpa procedure assuming higher modes as elastic to estimate seismic demands. *Earthquake Spectra*, 20(3):757–778.

Fahnestock, L., Sause, R., Ricles, J., Simpson, B., Kurata, M., Okazaki, T., Kawamata, Y., Tao, Z., Duke, J., Rivera, D., Astudillo, B., and Qie, Y. (2021). U.S.-Japan collaboration for shake table testing of a Frame-Spine system with Force-Limiting Connections. *17th WCEE World Conference on Earthquake Engineering: Sendai, Japan 2021*.

Flores, F., Charney, F., and Lopez-Garcia, D. (2016). The influence of gravity column continuity on the seismic performance of special steel moment frame structures. *Journal of Constructional Steel Research*, 118:217–230.

Fujimoto, M., Wada, A., Saeki, E., Takeuchi, T., and Watanabe, A. (1990). Development of unbonded brace. *Quarterly Column*, 115(1):91–96.

Heidebrecht, A. C. and Smith, B. S. (1973). Approximate analysis of tall wall-frame structures. *Journal of the Structural Division*, 99(2):199–221.

Ji, X., Kato, M., Wang, T., Hitaka, T., and Nakashima, M. (2009). Effect of gravity columns on mitigation of drift concentration for braced frames. *Journal of constructional steel research*, 65(12):2148–2156.

Khan, F. R. and Sbarounis, J. A. (1964). Interaction of shear walls and frames. *Journal of the Structural Division*, 90(3):285– 335.

Khatib, I. F., Mahin, S. A., and Pister, K. S. (1988). *Seismic behavior of concentrically braced steel frames*. Earthquake Engineering Research Center, University of California Berkeley . . . .

Lai, J.-W. and Mahin, S. A. (2015). Strongback System: A Way to Reduce Damage Concentration in Steel-Braced Frames. *Journal of Structural Engineering*, 141(9):04014223.

MacRae, G. A., Kimura, Y., and Roeder, C. W. (2004). Effect of column stiffness on braced frame seismic behavior. *Journal of Structural Engineering-asce*.

McKenna, F., Scott, M. H., and Fenves, G. L. (2010). Nonlinear Finite-Element Analysis Software Architecture Using Object Composition. *Journal of Computing in Civil Engineering*, 24(1):95–107.

Miranda, E. (1999). Approximate seismic lateral deformation demands in multistory buildings. *Journal of Structural Engineering*, 125(4):417–425.

P-695, F. (2009). *QUANTIFICATION OF BUILDING SEISMIC PERFORMANCE FACTORS.* Federal Emergency Management Agency.

Palermo, M., Laghi, V., Gasparini, G., and Trombetti, T. (2018). Coupled response of frame structures connected to a strongback. *Journal of Structural Engineering*, 144(9):04018148.

Qu, B., Sanchez-Zamora, F., and Pollino, M. (2014). Mitigation of inter-story drift concentration in multi-story steel concentrically braced frames through implementation of rocking cores. *Engineering Structures*, 70:208–217.

Qu, Z., Wada, A., Motoyui, S., Sakata, H., and Kishiki, S. (2012). Pin-supported walls for enhancing the seismic performance of building structures. *Earthquake engineering & structural dynamics*, 41(14):2075–2091.

Roeder, C. W. and Popov, E. P. (1978). Eccentrically braced steel frames for earthquakes. *Journal of the Structural Division*. Simpson, B. G. (2020). Higher-mode force response in multi-story strongback-braced frames. *Earthquake Engineering &*

Structural Dynamics, 49(14):1406–1427.

Simpson, B. G. and Mahin, S. A. (2018). Experimental and numerical investigation of strongback braced frame system to mitigate weak story behavior. *Journal of Structural Engineering*, 144(2):04017211.

Simpson, B. G. and Rivera Torres, D. (2021). Simplified Modal Pushover Analysis to Estimate First- and Higher-Mode Force Demands for Design of Strongback-Braced Frames. *Journal of Structural Engineering*, 147(12):04021196.

Slovenec, D., Sarebanha, A., Pollino, M., Mosqueda, G., and Qu, B. (2017). Hybrid testing of the stiff rocking core seismic rehabilitation technique. *Journal of Structural Engineering*, 143(9):04017083.

Takeuchi, T. and Suzuki, K. (2003). Performance-based design for truss-frame structures using energy dissipation devices. In *STESSA 2003*.

Tremblay, R. (2003). Achieving a stable inelastic seismic response for multi-story concentrically braced steel frames.

Watanabe, A., Hitomi, Y., Saeki, E., Wada, A., and Fujimoto, M. (1988). Properties of brace encased in buckling-restraining concrete and steel tube. In *Proceedings of ninth world conference on earthquake engineering*, volume 4, pages 719–724.

Wiebe, L. and Christopoulos, C. (2015). A cantilever beam analogy for quantifying higher mode effects in multistorey buildings. *Earthquake Engineering Structural Dynamics*, 44(11):1697–1716. 50 citations (Crossref) [2023-10-19].

Zhu, M., McKenna, F., and Scott, M. H. (2018). OpenSeesPy: Python library for the OpenSees finite element framework. *SoftwareX*, 7:6–11.